

Numerical Calculation of Internal Pressure Distribution of Vortex Flowmeter

Liang-Huai Tong¹, Xiu-Qin Chen², Jian Fan², Jin-Fu Li², Guo-Qing Zhao²,

1 Quzhou Special Equipment Inspection Center, Quzhou 324000, China;

2 College of Mechanical Engineering, Quzhou University, Quzhou, 324000, China;

ABSTRACT

As the most commonly used vortex flowmeter in flow monitoring and control, it plays an increasingly significant role in the industrial field. Therefore, in order to optimize the design of vortex flowmeter to meet the working requirements, this paper uses CFX calculation and simulation technology to study the flow of gas in the inner channel of vortex flowmeter, and analyzes the distribution of total pressure and static pressure in the inner channel of vortex flowmeter, so as to reveal the internal flow characteristics of vortex flowmeter and provide reference for the analysis of the working characteristics of vortex flowmeter. It is found that the gas flow in the vortex flowmeter is stable and the distributions of the total pressure and static pressure in the inner channel are reasonable. This study provides detailed data for the normal detection and control of the flow of vortex flowmeter.

Key words: *vortex flowmeter; simulation; pressure*

Date of Submission: 31-03-2020

Date of Acceptance: 18-04-2020

I. INTRODUCTION

The development and utilization of flow measurement devices have a more and more extensive impact on the development of industrialization and the improvement of national economy^[1], especially in the era of frequent industrial accidents and serious decline in energy reserves, the flow measurement devices are very important for the development of life^[2,3]. Vortex flowmeter is one of the most common measuring instruments for gas flow measurement. Many scholars have carried out theoretical and experimental research^[4,5] for it to improve continuously. He Linhan et al.^[6] made a detailed discussion on the influence of gas composition by analyzing the factors affecting the instrument error. Different gas compositions have different effects on flow measurement. It was found that the lower the content of different gas compositions in natural gas, the greater the relative density of gas, and the larger the flow when converted into standard condition. Desheng Chen^[7] used CFD numerical simulation to study the flow characteristics and measurement characteristics of vortex flowmeter under different flow conditions, such as uniform flow, disturbed flow and gas-liquid two-phase flow. Baoling Cui et al.^[8] carried out numerical simulation with RNG K- ϵ turbulence model by CFD and combined with experiments to study the vortex flowmeter with diameter of 150 mm, and pointed out that when the incidence angle of the swirler is 55°, the performance of the precession vortex flowmeter is the best. Caiwei Ma et al.^[9] studied the effect of the vibration of pipeline on the effective signal acquisition of vortex flowmeter, and put forward a sensor installation method to eliminate the vibration of pipeline of vortex flowmeter. By installing two sensors in parallel on the same side of the main body of flowmeter, and then applying difference disposal to the two channels of signals, the impact of pipeline vibration on signal acquisition was eliminated.

Different from the above research, this paper uses CFD^[10-13] to simulate the total pressure and static pressure inside the vortex flowmeter, predict the working performance of the vortex flowmeter in advance, and provide reference for the optimal design.

1 Calculation setting

1.1 Physical model

The basic parameters of the spinner are selected as shown in Fig.1.

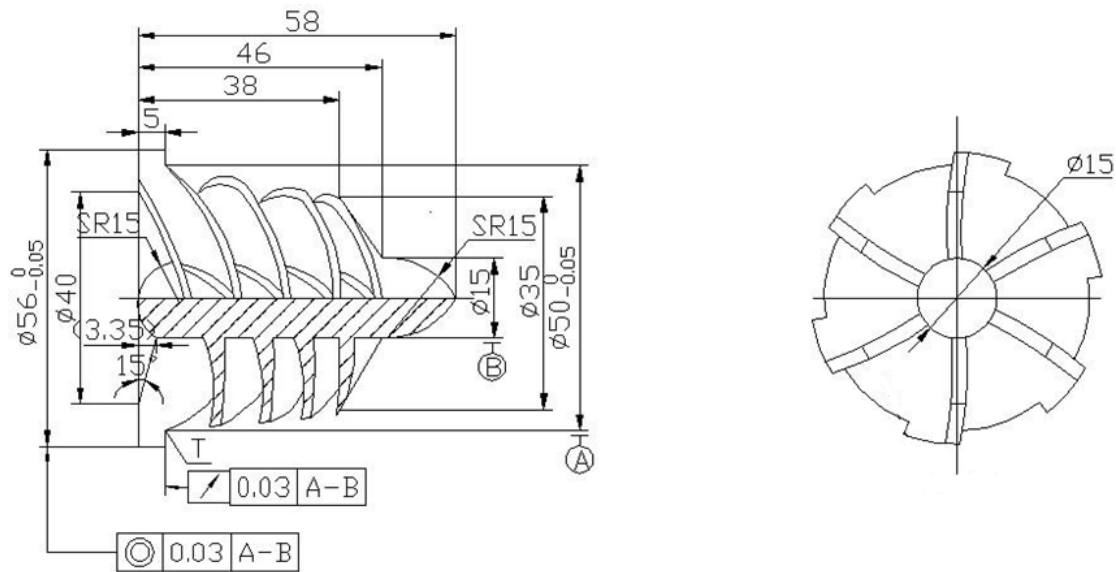


Fig. 1 Spinner

1.2 Grid division

After 3D digital modeling of vortex flowmeter with UG 3D software, the model file is imported into ICEM CFD in step format, and the whole model is processed in blocks and a new part is created at the same time. Considering the motion characteristics of the vortex flowmeter and the complexity of each part, the calculation domain of the whole vortex flowmeter is divided into eight parts by using the hybrid grid method. Mainly hexahedral mesh, with a total of 790000 meshes. The spinner grid is shown in Fig. 2 (a), the racer grid is shown in Fig. 2 (b), and the grid of the overall calculation domain is shown in Fig. 2 (c).

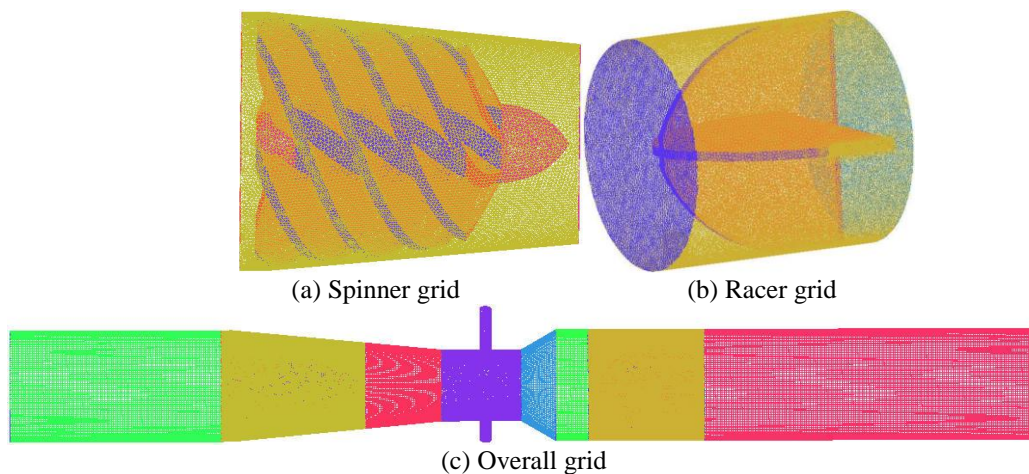


Fig.2 Grid of computing domain

II. RESULT ANALYSIS

The internal pressure distribution of the vortex flowmeter is analyzed under the conditions of the inlet flow of $10\text{m}^3/\text{h}$, $30\text{m}^3/\text{h}$, $60\text{m}^3/\text{h}$ and $90\text{m}^3/\text{h}$ respectively.

2.1 Total pressure distribution

(1) Horizontal middle section

Fig.3 (a) shows that when the inlet flow is $10\text{m}^3/\text{h}$, the lowest total pressure appears at the top of the spinner, with a value of -395Pa . The highest total pressure appears at the inlet, with a value of 384Pa . Fig.3 (b) shows that when the inlet flow is $30\text{m}^3/\text{h}$, the lowest total pressure appears at the top of the spinner, with a value of -1563Pa , and the highest total pressure appears at the inlet, with a value of 774Pa . Fig.3 (c) shows that when the inlet flow is $60\text{m}^3/\text{h}$, the lowest total pressure appears at the top of the spinner, with a value of -2342Pa , and the highest total pressure appears at the inlet, with a value of 1553Pa . Fig. 3 (d) shows that when the inlet flow is $90\text{m}^3/\text{h}$, the lowest total pressure appears at the top of the spinner, with a value of -3800Pa , and the highest total pressure appears at the inlet, with a value of 3500Pa .

It can be seen that after the gas enters into the contraction section, the vortex is formed at the top of the spinner under the influence of the spinner. Under any condition of inlet flow, a lower total pressure area will be formed at the top of the spinner, and the total pressure on both sides of the throat of the spinner is higher than that in the middle. The larger the inlet flow is, the lower the total pressure area on the top of the spinner is.

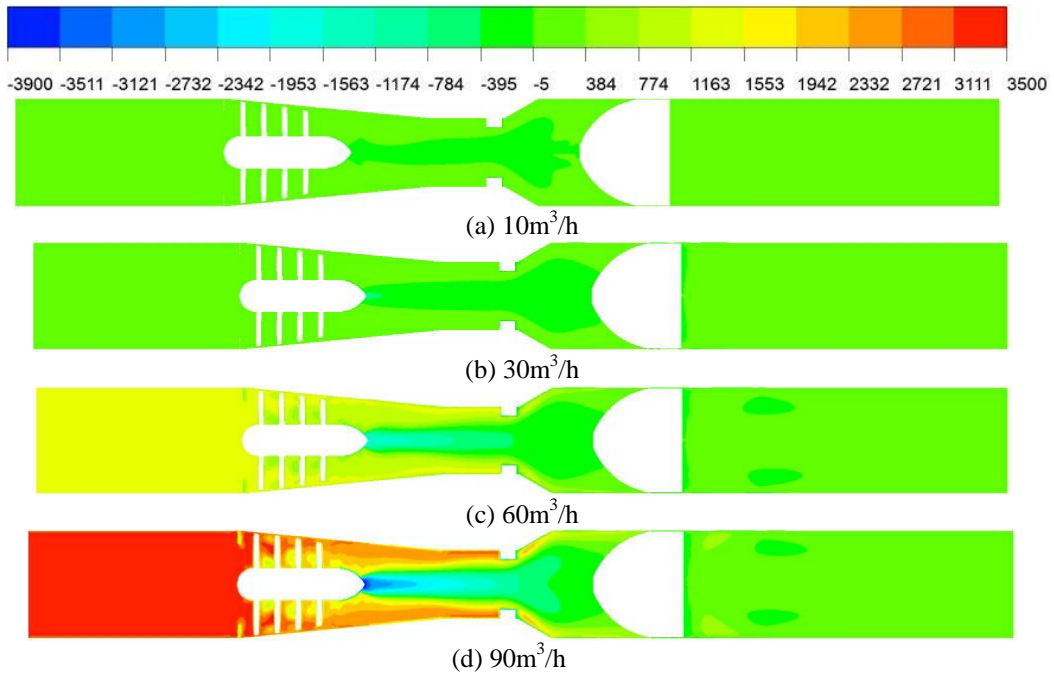
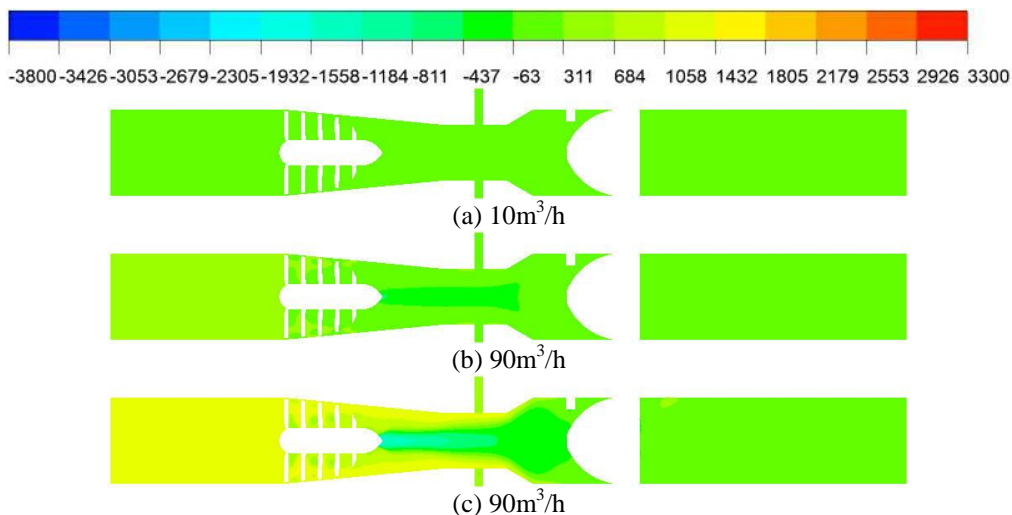


Fig. 3 Total pressure distribution of horizontal middle section (Pa)

(2) Vertical middle section

Fig.4 (a) shows that when the inlet flow rate is $10\text{m}^3/\text{h}$, the total pressure of each part in the flow passage does not change much, and its value is 311 Pa. Fig. 4 (b) shows that when the inlet flow is $30\text{m}^3/\text{h}$, the lowest total pressure appears at the top of the spinner, with a value of -437 Pa, and the highest total pressure appears at the inlet, with a value of 684 Pa. Fig.4 (c) shows that when the inlet flow is $60\text{m}^3/\text{h}$, the lowest total pressure appears at the top of the spinner, with a value of -2305 Pa, and the highest total pressure appears at the inlet, with a value of 684 Pa. Fig. 4 (d) shows that when the inlet flow is $90\text{m}^3/\text{h}$, the lowest total pressure appears at the top of the spinner, with a value of - 3800 Pa, and the highest total pressure appears at the inlet, with a value of 3300 Pa.

It can be seen that after the gas enters into the contraction section, the vortex is formed at the top of the spinner under the influence of the spinner. Under any condition of inlet flow, a lower total pressure area will be formed at the top of the spinner, and the total pressure on both sides of the throat of the spinner is higher than that in the middle. The larger the inlet flow is, the lower the total pressure area on the top of the spinner is.



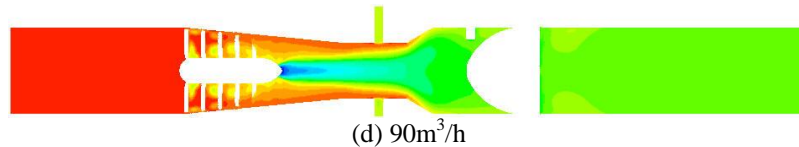


Fig. 4 Total pressure distribution of vertical middle section (Pa)

(3) Pressure sensing cross section

Fig. 5 (a) shows that when the inlet flow is $10\text{m}^3/\text{h}$, the total pressure value of each part of the cross section of the vortex flowmeter has little difference, and the value is -216 Pa . Fig. 5 (b) shows that when the inlet flow rate is $30\text{m}^3/\text{h}$, the highest total pressure appears on the wall of the flow passage, with a value of 495 Pa . The total pressure at the center is low and has little change, with a value of -453 Pa . Fig. 5 (c) shows that when the inlet flow is $60\text{m}^3/\text{h}$, the highest total pressure appears on the wall of the flow passage, with a value of 1442 Pa , and the total pressure at the center is low and has little change, with a value of -453 Pa . Fig. 5 (d) shows that when the inlet flow is $90\text{m}^3/\text{h}$, the highest total pressure appears on the wall of the flow passage, with a value of 3100 Pa , and the lowest total pressure appears at the center, with a value of -1400 Pa .

It can be seen that after the gas enters the throat of the spinner through the spinner, the air flow is affected by the spinner and the vortex is formed at the top of the spinner, and the core of the vortex moves near the center of the cross section. Under the condition of any inlet flow rate, the total pressure center of the flow passage in the vortex flowmeter is lower than that of the wall at the cross-section position, and the minimum total pressure center increases gradually outward along the diameter direction. The total pressure in the cross-section increases with the increase of the inlet flow rate. The total pressure near the channel wall rises significantly, while the total pressure at the center changes little and remains at a low value.

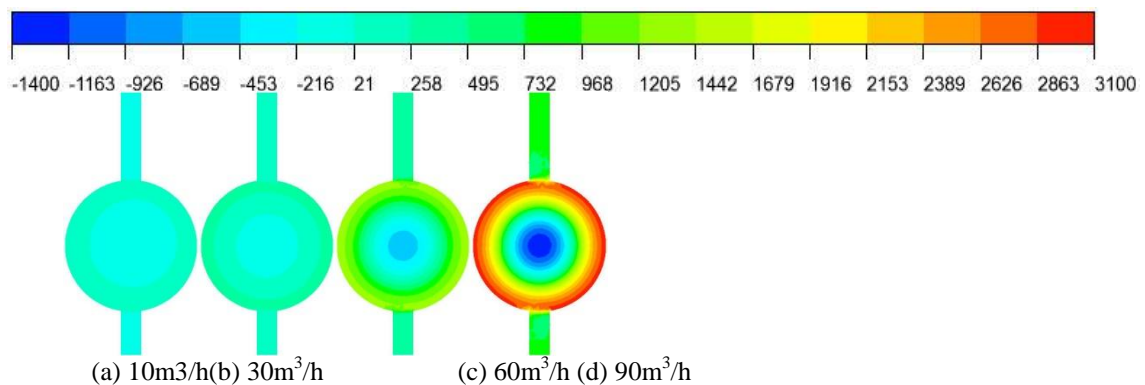


Fig.5 Total pressure distribution of pressure sensor cross section(Pa)

(4) Exit extension cross section

Fig. 6 (a) shows that when the inlet flow is $10\text{m}^3/\text{h}$, the total pressure value of each part of the cross section of the vortex flowmeter has little difference, and the value is -20 Pa . Fig. 6 (b) shows that when the inlet flow rate is $30\text{m}^3/\text{h}$, the highest total pressure appears on the wall of the flow passage, with a value of 89 Pa . The total pressure in the center is low and has little change, with a value of 35 Pa . There are four low-pressure areas around the center, with a value of 7 Pa . Fig. 6 (c) shows that when the inlet flow rate is $60\text{m}^3/\text{h}$, the highest total pressure appears on the wall of the flow passage, with a value of 308 Pa . The total pressure at the center is low and has little change, with a value of 89 Pa . There are four low-pressure areas around the center, with a value of -20 Pa . When the inlet flow is $90\text{m}^3/\text{h}$, the highest total pressure value appears on the wall of the flow passage, its value is 437 Pa , and the lowest total pressure appears in the center, its value is 117 Pa , four low-pressure areas appear around the center, its value is -20 Pa .

It can be seen that after the gas enters the throat through the spinner, the air flow is affected by the spinner and the vortex is formed at the top of the spinner, and the core of the vortex moves near the center of the cross section. Under the condition of any inlet flow, the total pressure at the outlet of center of the vortex flowmeter is lower than that of the wall at the cross section, and four low-pressure areas are formed at the center and increase gradually outward along the diameter direction. The total pressure in the cross-section increases with the increase of the inlet flow rate, and the total pressure near the channel wall rises significantly. The total pressure in the four low-pressure areas in the center changes little and remains at a low value.

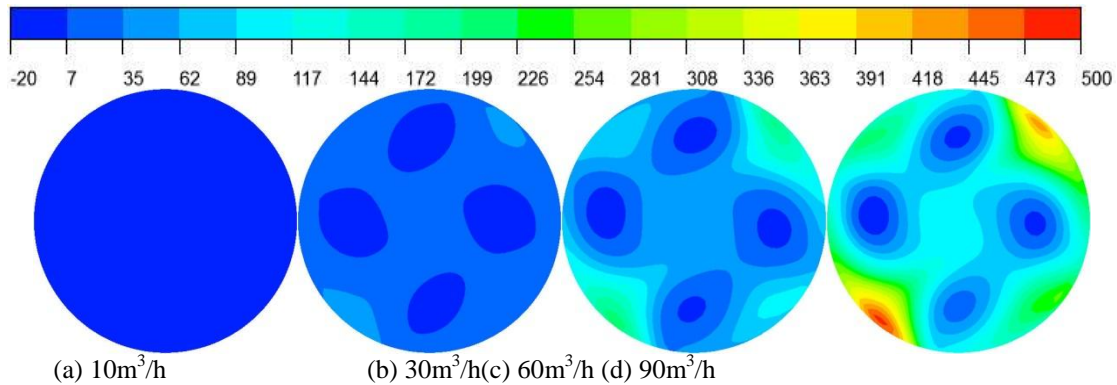


Fig. 6 Total pressure distribution of cross section of outlet extension (Pa)

(5) Top cross section of spinner

Fig. 7 (a) shows that when the inlet flow rate is $10\text{m}^3/\text{h}$, the total pressure value of each part of the cross section of the vortex flowmeter has little difference, and its value is 400 Pa. Fig. 7 (b) shows that when the inlet flow rate is $30\text{m}^3/\text{h}$, the highest total pressure appears at the wall of the flow channel, and its value is 400 Pa, and the total pressure is low at the center and has little change, with a value of -200 Pa. Fig. 7 (c) shows that when the inlet flow rate is $60\text{m}^3/\text{h}$, the highest total pressure appears on the wall of the flow passage, with a value of 1300 Pa. The total pressure is low at the center and has little change, with a value of -1400 Pa. Fig. 7 (d) shows that when the inlet flow is $90\text{m}^3/\text{h}$, the highest total pressure appears on the wall of the flow channel, with a value of 2800 Pa, and the lowest total pressure value appears in the center, with a value of -3200 Pa.

It can be seen that after the gas enters the throat through the spinner, the air flow is affected by the spinner and the vortex is formed at the top of the spinner, and the core of the vortex moves near the center of the cross section. Under the condition of any inlet flow rate, the total pressure of center of the flow passage in the vortex flowmeter is lower than that of the wall at the cross-section position, and the lowest total pressure center increases gradually outward along the diameter direction. The total pressure in the cross section increases with the increase of the inlet flow rate. The total pressure near the channel wall rises significantly, while the total pressure at the center changes little and remains at a low value.

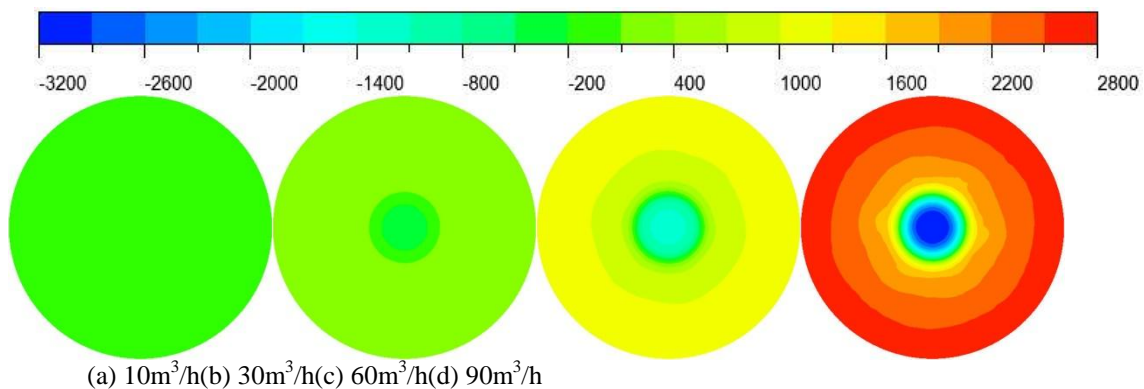


Fig. 7 Total pressure distribution of cross section at the top of spinner (Pa)

2.2 Static pressure distribution

(1) Horizontal middle section

Fig. 8 (a) shows that when the inlet flow is $10\text{m}^3/\text{h}$, the lowest static pressure appears at the top of the spinner, with a value of -385 Pa, and the highest static pressure appears at the inlet, with a value of 320 Pa. Fig. 8 (b) shows that when the inlet flow is $30\text{m}^3/\text{h}$, the lowest static pressure appears at the top of the spinner, with a value of -1563 Pa, and the highest static pressure appears at the inlet, with a value of 750 Pa. Fig. 8 (c) shows that when the inlet flow is $60\text{m}^3/\text{h}$, the lowest static pressure appears at the top of the spinner, with a value of -2742 Pa, and the highest static pressure appears at the inlet, with a value of 1500 Pa.

It can be seen that after the gas enters into the contraction section, the vortex is formed at the top of the spinner under the influence of the spinner. Under any condition of inlet flow, a lower static pressure area will be formed at the top of the spinner, and the static pressure on both sides of the throat of the spinner is higher than that in the middle. The larger the inlet flow is, the lower the value of the static pressure area on the top of the spinner is.

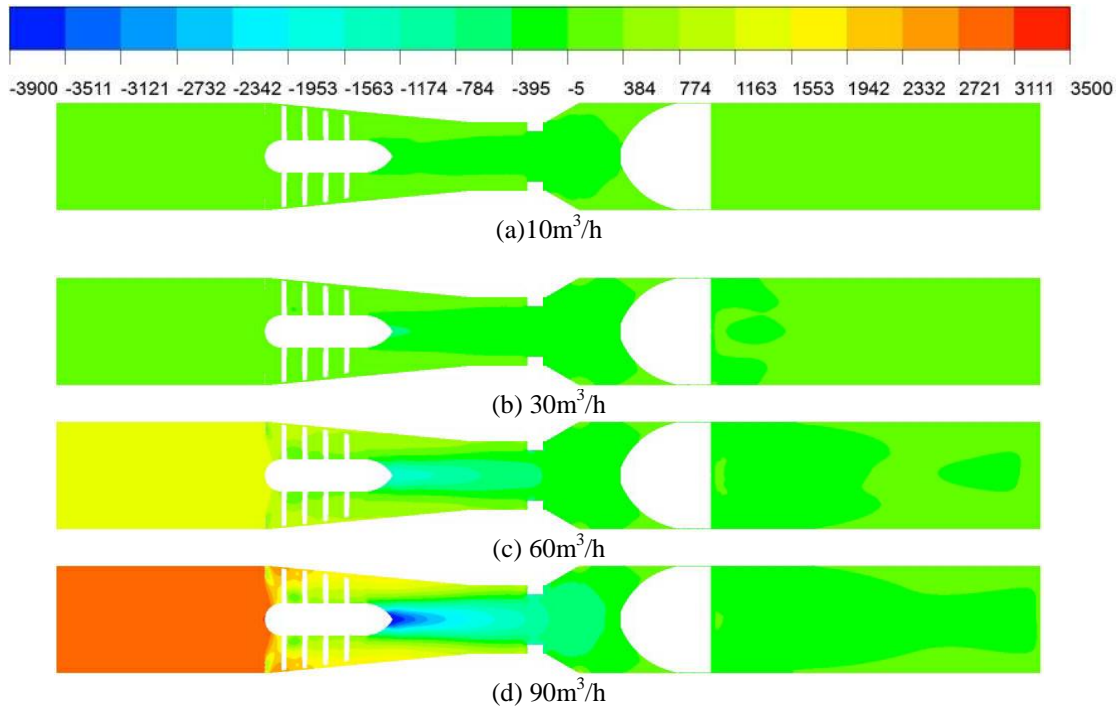


Fig. 8 Static pressure distribution of horizontal middle section (Pa)

(2) Vertical middle section

Fig. 9 (a) shows that when the inlet flow is $10\text{m}^3/\text{h}$, the total pressure of each part in the flow passage does not change much, and its value is 584 Pa . Fig. 9 (b) shows that when the inlet flow is $30\text{m}^3/\text{h}$, the lowest static pressure appears at the top of the spinner, and its value is -537 Pa , and the highest static pressure appears at the inlet, and its value is 958 Pa . Fig. 9 (c) shows that when the inlet flow is $60\text{m}^3/\text{h}$, the lowest static pressure appears at the top of the spinner, with a value of -2032 Pa . The highest static pressure appears at the inlet, with a value of 1332 Pa . Fig. 9 (d) shows that when the inlet flow is $90\text{m}^3/\text{h}$, the lowest total pressure appears at the top of the spinner, with a value of -3900 Pa , and the highest total pressure appears at the inlet, with a value of 3200 Pa .

It can be seen that after the gas enters into the contraction section, the vortex is formed at the top of the spinner under the influence of the spinner. Under any condition of inlet flow, a lower static pressure area will be formed at the top of the spinner, and the static pressure on both sides of the throat of the spinner is higher than that in the middle.

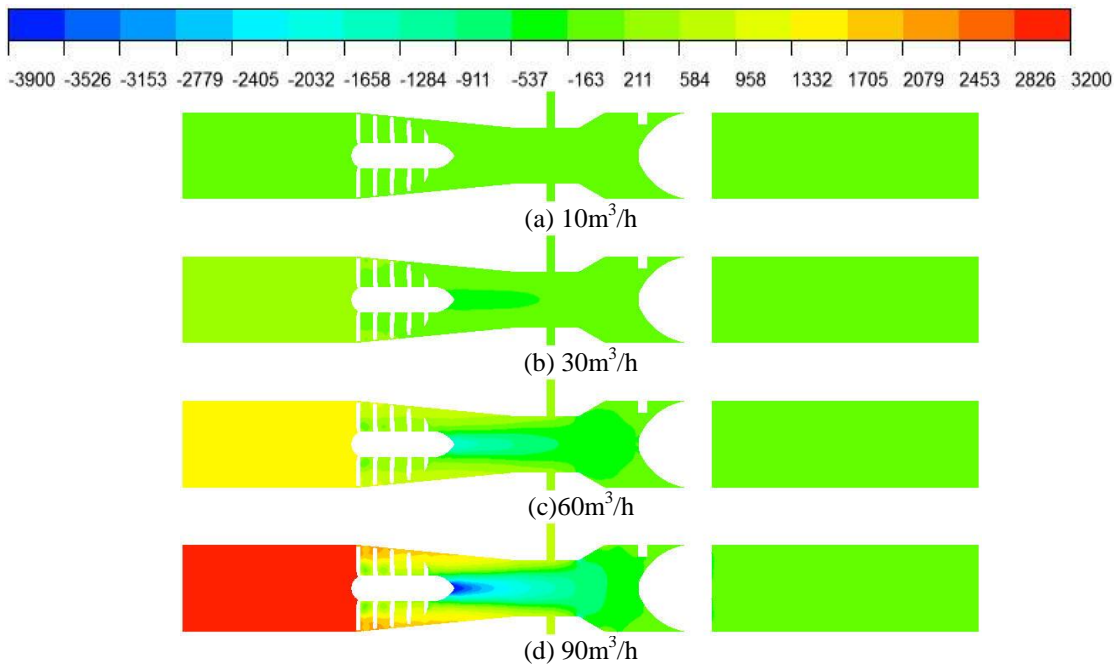


Fig. 9 Static pressure distribution of vertical middle section (Pa)

(3) Pressure sensing cross section

Fig. 10 (a) shows that when the inlet flow rate is $10\text{m}^3/\text{h}$, the static pressure value of each part of the cross section of the vortex flowmeter has little difference, and its value is 134 Pa. Fig. 10 (b) shows that when the inlet flow rate is $30\text{m}^3/\text{h}$, the highest static pressure value appears on the wall of the flow channel, with a value of 413 Pa, and the static pressure value of the central part is low and has little change, and its value is -842 Pa. Fig. 10 (c) shows that when the inlet flow rate is $60\text{m}^3/\text{h}$, the highest static pressure value appears on the wall of the flow passage, with a value of 553 Pa. The static pressure value at the center is low and has little change, with a value of -703 Pa. Fig. 10 (d) shows that when the inlet flow is $90\text{m}^3/\text{h}$, the highest static pressure value appears on the wall of the flow passage, with a value of 832 Pa, and the lowest static pressure value appears in the center, with a value of -1400 Pa.

It can be seen that after the gas enters the throat through the spinner, the air flow is affected by the spinner and the vortex is formed at the top of the spinner, and the core of the vortex moves near the center of the cross section. Under the condition of any inlet flow rate, the static pressure of center of inner flow channel of the vortex flowmeter is lower than that of the wall at the crosssection, and the static pressure center is the lowest and gradually increases outward along the diameter direction. The static pressure in the crosssection increases with the increase of the inlet flow rate, the static pressure near the channel wall rises significantly, and the static pressure at the center changes little and remains at a low value.

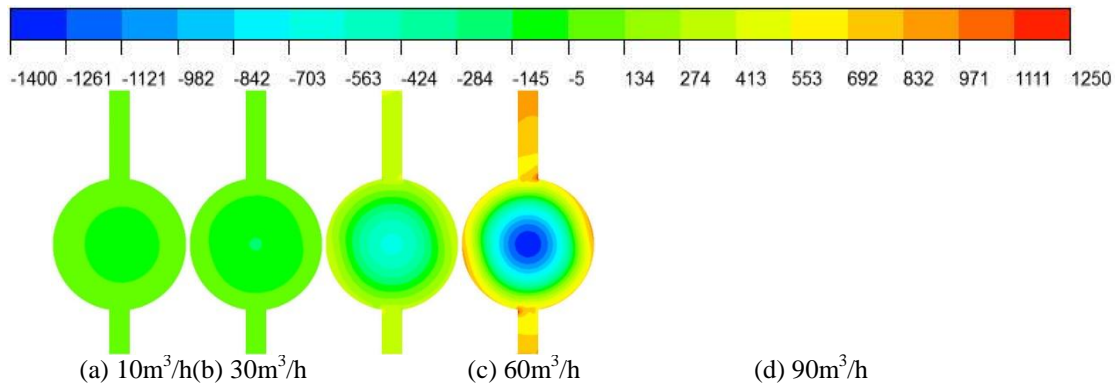


Fig. 10 Static pressure distribution of pressure sensing cross section (Pa)

(4) Exit extension cross section

Fig. 11 (a) shows that when the inlet flow is $10\text{m}^3/\text{h}$, the static pressure value of each part of the cross section of the vortex flowmeter has little difference, and the value is -3 Pa. Fig. 11 (b) shows that when the inlet flow rate is $30\text{m}^3/\text{h}$, the highest static pressure value appears on the wall of the flow passage, with a value of 8 Pa. The static pressure value at the center is low and has little change, with a value of -13 Pa. Four low-pressure areas appear around the center, with a value of -13 Pa. Fig. 11 (c) shows that when the inlet flow rate is $60\text{m}^3/\text{h}$, the highest static pressure value appears on the wall of the flow passage, with a value of 28 Pa. The static pressure value at the center is low and has little change, with a value of -13 Pa. Four low-pressure areas appear around the center, with a value of -29 Pa. Fig. 11 (d) shows that when the inlet flow rate is $90\text{m}^3/\text{h}$, the highest static pressure value appears on the wall of the flow passage, its value is 39 Pa, and the lowest static pressure value appears in the center.

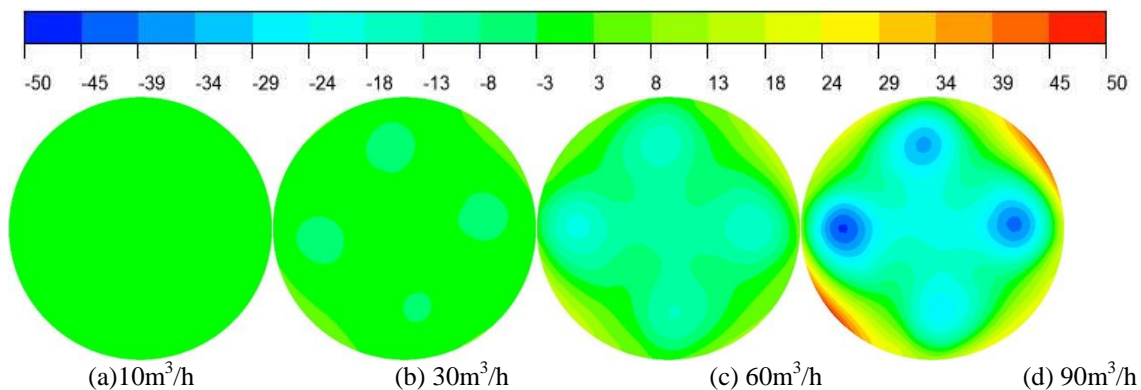


Fig. 11 Static pressure distribution of cross section of outlet extension (Pa)

(5) Top cross section of Spinner

Fig. 12 (a) shows that when the inlet flow is $10\text{m}^3/\text{h}$, the static pressure value of each part of the cross section of the vortex flowmeter has little difference, and the value is -200 Pa . Fig. 12 (b) shows that when the inlet flow rate is $30\text{m}^3/\text{h}$, the highest static pressure value appears on the wall of the flow passage, with a value of 400 Pa . The static pressure value at the center is low and has little change, with a value of -200 Pa . Fig. 12 (c) shows that when the inlet flow rate is $60\text{m}^3/\text{h}$, the highest static pressure value appears on the wall of the flow passage, with a value of 1000 Pa . The static pressure value at the center is low and has little change, with a value of -1500 Pa . Fig. 12 (d) shows that when the inlet flow is $90\text{m}^3/\text{h}$, the highest static pressure value appears on the wall of the flow passage, with a value of 2800 Pa , and the lowest static pressure value appears in the center, with a value of -3200 Pa .

It can be seen that after the gas enters the throat through the spinner, the air flow is affected by the spinner and the vortex is formed at the top of the spinner, and the core of the vortex moves near the center of the cross section. Under the condition of any inlet flow, the static pressure of center of the inner flow passage of the vortex flowmeter is lower than that of the wall at the crosssection position, and the lowest static pressure center is gradually increased outward along the diameter direction. The static pressure in the crosssection increases with the increase of the inlet flow rate, the static pressure near the channel wall rises significantly, and the static pressure at the center changes little and remains at a low value.

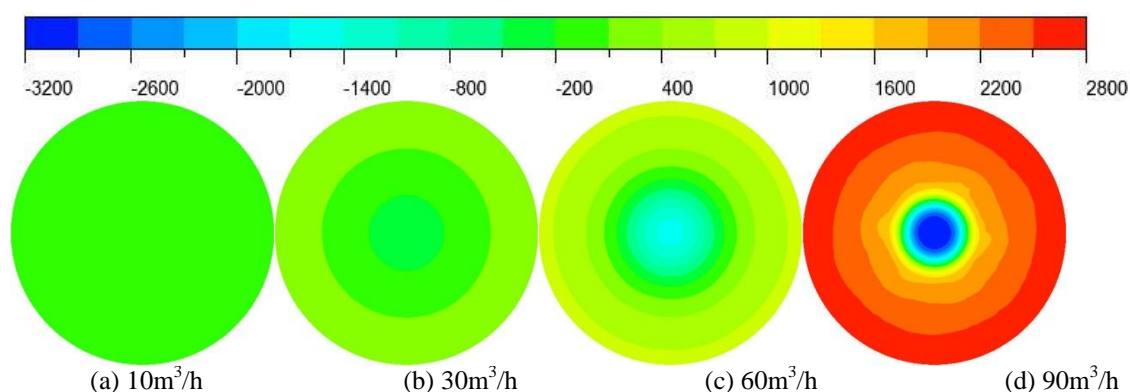


Fig. 12 Static pressure distribution of the top cross section of the spinner (Pa)

III. CONCLUSION

In this paper, the flow simulation software ICFM CFD and ANSYS CFX are used to analyze the working characteristics of the vortex flowmeter, and the distribution of the total pressure and the static pressure in each section of the inner channel of the vortex flowmeter are analyzed under different inlet velocity. It is found that the total pressure in the cross section increases with the increase of the inlet flow, the total pressure near the channel wall rises significantly, the total pressure at the center changes little and remains at a low value, and the larger the inlet flow is, the lower the value of the total pressure area at the top of the spinner is. The static pressure in the cross section increases with the increase of the inlet flow rate, and the static pressure near the channel wall rises significantly. The static pressure at the center changes little and keeps at a low value. Under any condition of inlet flow, a lower static pressure area will be formed on the top of the spinner, and the larger the inlet flow is, the lower the value of the static pressure area on the top of the spinner is, and the static pressure on both sides of the throat of the spinner is higher than that in the middle. The internal flow of the vortex flowmeter is stable, and the total pressure and static pressure distribution are reasonable. It conforms to the working principle and working conditions of the vortex flowmeter. It can work stably when the inlet flow is large or small.

ACKNOWLEDGEMENTS

The work was supported by Zhejiang Provincial Market Supervision and Administration Project (No. 20190131) and Quzhou Science and Technology Project (No. 2018K05).

REFERENCE

- [1]. Li Ziping. Development and Prospect of flow meters [J]. Science and technology wind, 2019, (19): 179.
- [2]. Shao Wen, song Limin, Zhang Wei. Selection and application analysis of domestic natural gas flowmeter [J]. PetroChina, 2015, (03): 62-64.
- [3]. Zhou Yan. Exploration on the application value of flow measurement in the field of energy measurement [J]. Instrument standardization and measurement, 2019, (02): 42-43, 48.
- [4]. Srinivasan Dattarajan, Shishir Pali, Neville Fernandes. Measurement of steam quality using a vortex flowmeter [J]. Flow Measurement and Instrumentation, 2018, 65: 3.

- [5]. Xiliang. Uncertainty analysis of measurement results of Precession Vortex Flowmeter [J]. Instrument standardization and measurement, 2018, (01): 45-48.
- [6]. He Linhan, Liu Qian. Influence of gas composition on the measurement of Precession Vortex Flowmeter [J]. Chemical engineering and equipment, 2019, (10): 146-147.
- [7]. Chen Desheng. Influence of inlet flow conditions on measurement characteristics of Precession Vortex Flowmeter [D]. Zhejiang: Zhejiang University of technology, 2018.
- [8]. Cui Baoling, LV Ziqiang, Chen Desheng. Effect of incidence angle of Spinner on performance of Precession Vortex Flowmeter [J]. Journal of agricultural engineering, 2015, 31(02): 53-58.
- [9]. Ma Caiwei, Zhao Xinhua. Experimental study on anti vibration interference of Precession Vortex Flowmeter Based on difference method [J]. Journal of Tianjin University of technology, 2014, 30(05): 6-8, 16.
- [10]. Zhang hang, Fu Junfeng, Wang Haijun. Selection of grid generation method for cross pipe flow field based on ICEM CFD [J]. China water transport, 2019, 19(10): 230-231.
- [11]. Su Yechun, Wu Peifeng. Application of ICEM CFD structured grid in pumping station engineering [J]. Jiangsu water conservancy, 2017, (01): 13-16.
- [12]. Li Lei. Translation practice report of ANSYS fluid technology software release notes [D]. Shanghai: Shanghai Normal University, 2019.
- [13]. Feng Tianyu. Fluid test and data analysis of cooling water pump based on ANSYS CFX [J]. Equipment manufacturing technology, 2017, (10): 26-27, 44.

Liang-Huai Tong,etal "Numerical Calculation of Internal Pressure Distribution of Vortex Flowmeter." *The International Journal of Engineering and Science (IJES)*, 9(4) (2020): 34-42.